RSC Advances

PAPER

View Article Online
View Journal | View Issue

Cite this: *RSC Adv.*, 2018, **8**, 30468

Design and synthesis of N-substituted perylene diimide based low band gap polymers for organic solar cell applications†

Savita Meena,[a] Tauheed Mohammad,[b] Viresh Dutta[b] and Josemon Jacob *[a]

In this study, we report on the synthesis and device studies of a series of new copolymers containing N-substituted perylene dimide and dioctylfluorene units as part of the main backbone. A facile synthetic approach avoiding non-selective bromination was used to synthesize the monomer **M1** by the reaction of perylene-3,4,9,10-tetracarboxylic dianhydride with 2-amino-7-bromo-9,9-dioctylfluorene. The copolymers **P1** and **P2** were synthesized by Suzuki polycondensation of **M1** with 2,2′-(9,9-dioctyl-9*H*-fluoren-2,7-diyl)bis(4,4,5,5-tetramethyl-1,3,2-dioxaborolane) **M2** and 9-(heptadecan-9-yl)-2,7-bis(4,4,5,5-tetramethyl-1,3,2-dioxaborolan-2-yl)-9*H*-carbazole **M3**, respectively. The copolymer **P3** was synthesized by direct arylation polymerization of **M1** with 4,7-bis(4-octylthiophen-2-yl)benzo[*c*]-1,2,5-thiadiazole **M4**. All the copolymers showed thermal stability greater than 380 °C as evidenced from thermogravimetric analysis. The copolymers exhibited a narrow optical band gap (1.80–2.08 eV) with their UV-visible absorption spectra extending up to the NIR region and they are found to be suitable for use in OSC applications. The molecular weights of the polymers **P1–P3** were found to be in the range of 10.68 to 16.02 kg mol^{-1} as measured from GPC analysis. The surface morphology of the active layers based on **P1**/**P2**/**P3**:P3HT blend films was investigated by AFM and the rms values from height images range from 0.65 to 2.90 nm. The polymers were blended with P3HT to fabricate BHJ solar cells in three different weight ratios *i.e.* 1 : 1, 1.5 : 1 and 2 : 1 and the best power conversion efficiency was observed for the binary film of **P3**:P3HT blend device in a 1 : 1 weight ratio which reached up to 1.96% with a V_{oc} of 0.55 V, J_{sc} of 10.12 mA cm^{-2} and FF of 34.63% which is among the highest reported for BHJ solar cells with N-substituted PDI based acceptors.

Received 19th June 2018
Accepted 20th August 2018

DOI: 10.1039/c8ra05232h

rsc.li/rsc-advances

Introduction

Organic solar cells (OSCs) are a promising alternative to the inorganic silicon based devices due to their low cost, ease of fabrication, flexibility and light weight.[1,2] During the past decade, fullerene and its derivatives have been extensively investigated as electron acceptors for OSCs, $PC_{61}BM$ and $PC_{71}BM$ in particular.[3] However, these acceptors suffer from some drawbacks such as limited light absorption in the visible region, high cost, instability of surface morphology in the blend films, difficulty in synthesis and purification and limited energy level tunability.[4,5] To overcome these challenges, there has been lot of reports in the recent literature on the design of non-fullerene based acceptors[6,7] with broader absorption, readily tunable energy levels, and ease of synthesis and purification.[8,9] Solution processable, non-fullerene bulk heterojunction (BHJ) solar cells with power conversion efficiencies (PCEs) > 8% have recently been reported which indicate the potential of non-fullerene electron acceptors.[10,11]

Perylene diimides (PDIs) are the most widely studied class of non-fullerene acceptors in OSCs[12,13] because of their large electron mobility with probable generation of a highly conducting path along their π–π stacking axis due to their strong tendency to form ordered aggregates and low-lying frontier energy levels.[14] PDIs are also advantageous due to their high absorption ability, high photochemical and optical stability, reversible redox properties, ease of synthetic modification and excellent environmental/thermal stability.[15–17] PDI based molecules and polymers have progressively attracted significant attention in applications such as light-emitting diodes,[18] sensors,[19] organic field-effect transistors,[20,21] light-harvesting arrays,[22] molecular wires,[23] photochromic materials[24] and photovoltaic cells.[25,26] Further, in PDI unit, the optical, electrochemical and charge transport properties can be tailored by introduction of appropriate substituents at the N-positions[26,27]

[a]*Department of Materials Science and Engineering, Indian Institute of Technology Delhi, Hauz Khas, New Delhi-110016, India. E-mail: jacob@polymers.iitd.ac.in; Tel: +91-11-26591425*

[b]*Photovoltaic Laboratory, Centre for Energy Studies, Indian Institute of Technology Delhi, Hauz Khas, New Delhi-110016, India*

† Electronic supplementary information (ESI) available. See DOI: 10.1039/c8ra05232h

or at the perylene bay positions,[28,29] offering wider scope for tuning the optical as well as processing properties.[30]

Janssen and co-workers were the first to demonstrate the use of N-substituted PDI based polymers in OSCs.[31] Mikroyannidis *et al.*[32] synthesized alternating phenylenevinylene copolymer with PDI moiety along the backbone by Heck coupling reaction for use as an acceptor in OSCs. This copolymer acts as an n-type organic semiconductor with electron mobility of $\sim 0.85 \times 10^{-2}$ cm^{-2} V^{-1} s^{-1}. A blend device consisting of the above acceptor copolymer and a poly(3-phenyl hydrazonethiophene) donor resulted in a PCE of 1.67% that further increased to 2.32% by thermal treatment and reported one of the best efficiency for N-substituted PDI polymers. In 2011, Z. Liang *et al.*[33] developed a variety of photo stable polymers containing poly(ethylene glycol) or poly(propylene glycol) segments in the N-substituted PDI backbone and used as acceptor in a PSC with poly(3-hexylthiophene) (P3HT) as donor. The polymer/P3HT (1 : 1 ratio) blend device gave a PCE of 0.1% with low J_{sc} of only 0.6 mA cm^{-2}. The low performance was attributed to the improper film morphology and low charge transport in the polymer blend. W. Fu *et al.*,[34] Jin *et al.*[35] and Koyuncu *et al.*[36] have recently demonstrated the use of PDI based polymers as acceptor material in BHJ solar cells with moderate power conversion efficiency.

The N-substitution at imide position of PDI can affect the solubility and molecular packing of the polymer in the solid state, without influencing the conjugation effect of the PDI backbone and thus the opto-electrochemical properties. In our efforts to develop PDI based acceptors for use in BHJ solar cells, we herein describe the synthesis of a novel N-substituted PDI based monomer and its alternating donor and acceptor type copolymers containing flourene, carbazole and thiophene–benzothiadiazole–thiophene moieties with tunable electrochemical and optical properties and examine their performances in OSCs. In this work, we report the synthesis of three new polymers **P1**, **P2** and **P3** obtained either by Suzuki or direct arylation polymerization reactions.[37,38] The optical, electrochemical properties and OSCs application of these copolymers were carefully investigated and correlated with their chemical structures.

Experimental

Materials

The solvents dimethylsulfoxide (DMSO), dimethyl acetamide, chloroform ($CHCl_3$), methanol (CH_3OH), acetone, 1,4-dioxane, tetrahydrofuran (THF) and toluene were dried and distilled by well known standard procedures[39] and kept in a glovebox for further use. Fluorene (**1**), 4,7-dibromobenzo[*c*]-1,2,5-thiadiazole (**7**), 9-(heptadecan-9-yl)-2,7-bis(4,4,5,5-tetramethyl-1,3,2-dioxaborolan-2-yl)-9*H*-carbazole (**M3**) and perylene-3,4,9,10-tetracarboxylic dianhydride were purchased from Sigma-Aldrich (USA) and was used directly without purification. 2-Bromo-9,9-dioctylfluorene (**2**), 2-bromo-7-nitro-9,9-dioctylfluorene (**3**), 2-amino-7-bromo-9,9-dioctylfluorene (**4**), 2,7-dibromo-9,9-dioctyl-9*H*-fluorene (**5**) and 4,4,5,5-tetramethyl-2-(4-octylthiophene-2-yl)-1,3,2-dioxaborolane (**6**) were synthesized by reported literature procedures.[40–42] 2,2′-(9,9-Dioctyl-9*H*-fluoren-2,7-diyl)bis(4,4,5,5-tetramethyl-1,3,2-dioxaborolane) (**M2**) and 4,7-bis(4-octylthiophen-2-yl)benzo[*c*]-1,2,5-thiadiazole (**M4**) were synthesized by reported methods with modified reaction conditions and improved yields[43,44] (details were given in ESI†).

General measurements and characterization

The monomers were analysed for C, H and N using a Perkin-Elmer 2400 Series II elemental analyser. The ^1H and ^{13}C NMR spectral data were recorded on a Bruker spectrospin DPX-400 spectrometer operating at 400.13 MHz and 100.61 MHz, respectively. The chemical shifts are referenced to $CDCl_3$ solvent (7.26 and 77.0 ppm for ^1H and ^{13}C NMR, respectively) relative to tetramethylsilane (TMS). Fourier transform infrared (FT-IR) spectra were obtained on KBr disks in the range of 4000–450 cm^{-1} using a Thermo Scientific Nicolet 6700 FT-IR spectrometer. Ultraviolet-visible spectra were measured in solution and in film on a Perkin-Elmer Lambda 1050 UV-visible spectrophotometer. Thermogravimetric analysis (TGA) was performed on a Perkin Elmer Pyris 6 thermal analysis system under N_2 atmosphere at a heating rate of 20 °C min^{-1}. The molecular weight determination was carried out on a Waters series 1515 gel permeation chromatograph (GPC) equipped with WATERS 1515 column. The measurement was performed using THF as eluent at a flow rate of 0.5 mL min^{-1} at 30 °C and samples were prepared in THF (1 mg mL^{-1}). The number-average molecular weight (M_n), weight-average molecular weight (M_w) and dispersities ($D = M_w/M_n$) of the polymers were determined using calibration curves obtained from polystyrene standards. Cyclic voltammograms (CV) for electrochemical properties were recorded by using a Zehnar Zehnnium potentiostat-galvanostat instrument with a glassy carbon working electrode, a platinum counter electrode and a Ag/AgCl reference electrode. The surface morphology of the blended films was investigated by atomic force microscopy (AFM) using a Nanoscope Bruker icon dimension with scan Asyst in the tapping mode. MALDI-TOF MS spectrum of **M1** was recorded on an ultraflextreme Bruker Daltonics TOF system in HCCA matrix.

Synthetic procedures for synthesis of monomer and polymers

Monomer synthesis

*Synthesis of 2,9-bis(7-bromo-9,9-dioctyl-9H-fluoren-2-yl)anthrax[2,1,9-def:6,510-d,e,f′]diisoquinoline-1,3,8,10(2H,9H)tetraone (**M1**).* Perylene-3,4,9,10-tetracarboxylic dianhydride (1.0 g, 2.54 mmol), **4** (2.5 g, 5.16 mmol), anhydrous zinc acetate (0.42 g, 2.25 mmol) and imidazole (5.0 g, 73.44 mmol) were stirred under N_2 atmosphere first at 100 °C for 12 h and then at 160 °C for an additional 12 h. The progress of the reaction was monitored by thin layer chromatography (TLC) using $CHCl_3$. The reaction mixture was then allowed to cool to *ca.* 80 °C and poured into 150 mL of 1 N aqueous hydrochloric acid solution. The red brown precipitate was filtered and washed sequentially with 0.5 N HCl (2 × 20 mL), distilled water (2 × 20 mL) and CH_3OH (3 × 20 mL). The solid was dissolved in $CHCl_3$ (30 mL), washed with distilled water (30 mL) and dried over anhydrous Na_2SO_4.

The solvent was evaporated on a rotary evaporator and the crude product was purified by column chromatography (silica gel, $CHCl_3$) to obtain **M1** as a red brown solid. Yield: 3.0 g, 90%. Anal. calc. for $C_{82}H_{88}N_2O_4Br_2$: C, 74.31%; H, 6.69%; N, 2.11%. Found: C, 74.61%; H, 6.47%; N, 2.21%. ^{1}H NMR (400.13 MHz, $CDCl_3$, 25 °C *vs.* TMS) δ: 8.73 (d, 4H, $J = 8.0$ Hz) 8.61 (d, 4H, $J = 8.0$ Hz) 7.83 (d, 2H, $J = 8.0$ Hz) 7.61 (d, 2H, $J = 8.0$ Hz) 7.51–7.49 (m, 4H) 7.37–7.33 (m, 4H) 2.03–1.90 (m, 8H) 1.26–1.11 (m, 40H) 0.84 (t, 12H, $J = 7.2$ Hz) 0.72 (m, 8H). ^{13}C NMR (100.61 MHz, $CDCl_3$, 25 °C *vs.* TMS) δ: 162.1, 152.4, 150.3, 139.3, 138.3, 133.1, 133.0, 130.2, 129.1, 128.1, 126.7, 125.3, 124.9, 122.6, 122.4, 122.0, 120.4, 119.4, 54.6, 38.8, 30.8, 28.9, 28.6, 28.2, 28.1, 22.7, 21.6, 13.1. MALDI-TOF MS: calc. for $C_{82}H_{88}N_2O_4Br_2$: 1325.40; found 1325.58 (M^+). FT-IR (KBr disk, ν_{max}/cm^{-1}): 2925, 2852, 1705, 1664, 1593, 1458, 1354, 1253, 1062, 796, 653. UV-vis spectrum λ_{max}(THF)/nm: 455, 485 and 520.

Polymers synthesis

*Synthesis of poly[2,9-bis(9,9-dioctyl-9H-fluoren-2-yl)anthra [2,1,9-def:6,5,10-d′e′f′]diisoquinoline-1,3,8,10(2H,9H)-tetraone-alt-9,9-dioctyl-9H-fluorene] (**P1**).* **M1** (0.20 g, 0.15 mmol), **M2** (0.10 g, 0.15 mmol), potassium carbonate (0.13 g dissolved in 0.45 mL of distilled water), $Pd(PPh_3)_4$ (3.48 mg, 2 mol%) and a phase transfer catalyst Aliquat 336 (3 drops) were added to N_2 purged mixture of water : toluene (1 : 6) (1.75 mL). The mixture was refluxed at 100 °C with stirring for 48 h under N_2 atmosphere and then an end capping agent, bromobenzene (0.79 μL, 5 mol%) was added to the mixture and heated for an additional 6 h followed by addition of phenyl boronic acid (0.92 mg, 5 mol%) with further heating for an additional 6 h. The reaction mixture was cooled to room temperature and poured drop wise into CH_3OH (200 mL) to precipitate out the polymer. The polymer was isolated by filtration and purified by Soxhlet extraction with CH_3OH, acetone and $CHCl_3$ successively. The polymer extract from $CHCl_3$ was concentrated on a rotary evaporated and reprecipitated from CH_3OH (100 mL). The dried polymer **P1** was obtained as a red brown solid. Yield: 0.19 g, 81%. ^{1}H NMR (400.13 MHz, $CDCl_3$, 25 °C *vs.* TMS) δ: 8.70 (br, 4H) 8.54 (br, 4H), 7.84–7.69 (br, 12H) 7.49–7.38 (br, 6H) 2.05–1.85 (br, 12H) 1.15 (br, 72H) 0.83 (br, 18H). FT-IR (KBr disk, ν_{max}/cm^{-1}): 2926, 2853, 1705, 1668, 1593, 1462, 1352, 1253, 1120, 813, 745. UV-vis spectrum λ_{max}(film)/nm: 341, 502 and 951. GPC analysis (PS standard): $M_w = 14.77$ kg mol^{-1}. Dispersity ($Đ$): 1.53.

*Synthesis of poly[2,9-bis(9,9-dioctyl-9H-fluoren-2-yl)anthra [2,1,9-def:6,5,10-d′e′f′]diisoquinoline-1,3,8,10(2H,9H)-tetraone-alt-9-(heptadecan-9-yl)-9H-carbazole] (**P2**).* **P2** was synthesized by a similar procedure as for **P1** using **M1** (0.20 g, 0.15 mmol), **M3** (0.10 g, 0.15 mmol), potassium carbonate (0.13 g dissolved in 0.45 mL of distilled water), $Pd(PPh_3)_4$ (3.48 mg, 2 mol%), phase transfer catalyst Aliquat 336 (3 drops), water : toluene (1 : 6) (1.75 mL), bromobenzene (0.79 μL, 5 mol%) and phenyl boronic acid (0.92 mg, 5 mol%). **P2** was obtained as a brown solid. Yield: 0.18 g, 77%. ^{1}H NMR (400.13 MHz, $CDCl_3$, 25 °C *vs.* TMS) δ: 8.72 (br, 4H) 8.56 (br, 4H) 8.20–7.71 (br, 12H) 7.52–7.29 (br, 6H) 4.69 (s, 1H) 2.05–1.68 (br, 12H) 1.18 (br, 72H) 0.83 (br, 18H). FT-IR (KBr disk, ν_{max}/cm^{-1}): 2924, 2852, 1704, 1669, 1564, 1457, 1351, 1261, 1093, 1019, 865, 700. UV-vis spectrum λ_{max}(film)/nm: 354, 516 and 954. GPC analysis (PS standard): $M_w = 10.68$ kg mol^{-1}. Dispersity ($Đ$): 1.28.

*Synthesis of poly[2,9-bis(9,9-dioctyl-9H-fluoren-2-yl)anthra [2,1,9-def:6,5,10-d′e′f′]diisoquinoline-1,3,8,10(2H,9H)-tetraone-alt-4,7-bis(4-octylthiophen-2-yl)benzo[c][1,2,5]thiadiazole] (**P3**).* Pivalic acid (4.62 mg, 30 mol%) and caesium carbonate (0.12 g, 0.38 mmol) were added to a mixture of **M1** (0.20 g, 0.15 mmol) and **M4** (0.08 g, 0.15 mmol) in anhydrous *N*,*N*-dimethylacetamide (1.5 mL, 0.1 M) with constant stirring at room temperature. The reaction mixture was purged with N_2 for 15 minutes, followed by addition of palladium acetate (3.39 mg, 10 mol%). The reaction mixture was heated at 100 °C for 72 h under N_2 atmosphere which was then cooled to room temperature and poured drop wise into cold CH_3OH (200 mL) to precipitate the polymer. The isolated polymer was further purified by using Soxhlet extraction steps similar to that of **P1**. The polymer collected in $CHCl_3$ was concentrated and precipitated from CH_3OH (100 mL) again, to get **P3** as a dark red brown solid. Yield: 0.19 g, 75%. ^{1}H NMR (400.13 MHz, $CDCl_3$, 25 °C *vs.* TMS) δ: 8.63 (br, 4H) 8.50 (br, 4H) 8.02 (br, 2H) 7.76 (br, 4H) 7.53–7.43 (br, 8H) 7.18 (br, 2H) 2.62 (br, 4H) 1.89–1.64 (br, 8H) 1.18 (br, 72H) 0.76 (br, 18H). FT-IR (KBr disk, ν_{max}/cm^{-1}): 2920, 2852, 1705, 1663, 1580, 1456, 1353, 1261, 1092, 1023, 866, 802, 695. UV-vis spectrum λ_{max}(film)/nm: 329, 520, 784 and 878. GPC analysis (PS standard): $M_w = 16.02$ kg mol^{-1}. Dispersity ($Đ$): 1.29.

Fabrication of organic solar cell devices

Poly(3,4-ethylenedioxythiophene):poly(styrenesulfonate) (PEDOT:PSS), regioregular poly(3-hexylthiophene) (P3HT) and 1,2-dichlorobenzene (DCB) were purchased from Sigma-Aldrich and used without further purification. PEDOT:PSS was filtered through 0.45 μm PVDF filter before use. The active layer was prepared by mixing **P1**, **P2** or **P3** and P3HT in three different weight ratios of 1 : 1, 1.5 : 1 and 2 : 1 in DCB and all solutions were filtered through a 0.45 μm PTFE filter before use. PSCs were fabricated with a structure of ITO/PEDOT:PSS/polymer/P3HT/Al using a standard solution processing method. Patterned indium tin oxide (ITO)-coated glass substrates were cleaned using labolene soap solution, deionized water, acetone and isopropyl alcohol with ultrasonic treatment each for 30 minutes at 50 °C. The cleaned ITO substrates were nitrogen dried and preheated in an oven at 100 °C for 60 minutes before oxygen plasma treatment for 15 minutes. A layer of PEDOT doped with PSS was spin-coated (3500 rpm for 45 seconds) on cleaned ITO surface, followed by annealing at 150 °C for 30 minutes. Then active layer of blend solution of P3HT:**P1** or **P2** or **P3** (new accepters) in DCB was spin casted (1000 rpm for 30 seconds) on the top of PEDOT:PSS layer and then annealed at 150 °C for 10 minutes. At the end, aluminium electrode (100 nm) was deposited through a shadow mask using thermal evaporation on top of the photoactive layer. All the devices were fabricated and tested in air without any encapsulation. *J*–*V* characteristics of PSCs were measured using a Keithley 2440 source meter, under AM 1.5 G illumination of Oriel Sol 3A class AAA solar simulator. The simulator was calibrated using a NREL certified Si solar cell.

Results and discussion

Synthesis and characterization of monomers and polymers

The synthetic approach toward the monomer, **M1** is shown in Scheme 1, whereas for **M2** and **M4** are shown in Scheme S1.† The synthesis of the target monomers 2,9-bis(7-bromo-9,9-dioctyl-9*H*-fluoren-2-yl)anthrax[2,1,9-def:6,510-d,e,f′]diisoquinoline-1,3,8,10(2*H*,9*H*)tetraone (**M1**), 2,2′-(9,9-dioctyl-9*H*-fluoren-2,7-diyl)bis(4,4,5,5-tetramethyl-1,3,2-dioxaborolane) (**M2**) and 4,7-bis(4-octylthiophen-2-yl)benzo[*c*]-1,2,5-thiadiazole (**M4**) were carried out as follows: in the first step bromination followed by alkylation of fluorene **1** in presence of N-bromosuccinimide (NBS) and *n*-octyl bromide, respectively, yielded 2-bromo-9,9-dioctylfluorene **2** (90%) which on nitration in the second step followed by reduction gave 2-amino-7-bromo-9,9-dioctylfluorene **4** in 74% overall yield.[40] Reaction of **4** with perylene-3,4,9,10-tetracarboxylic dianhydride in the presence of imidazole and anhydrous zinc acetate on heating at 160 °C under N_2 atmosphere resulted in **M1** in 90% yield. Bromination of **1** in presence of bromine gave dibromofluorene which on alkylation with *n*-octyl bromide using tetrabutylammonium hydroxide at 80 °C gave 2,7-dibromo-9,9-dioctyl-9*H*-fluorene **5** in 90% yield.[45] Reaction of **5** in presence of $Pd(dppf)Cl_2$ and potassium acetate with bis(pinacolato)diboron under N_2 atmosphere at 105 °C resulted in **M2** (70% yield). Reaction of **7** with **6** in toluene/THF under N_2 atmosphere in presence of sodium carbonate, $Pd(PPh_3)_4$ and tetrabutylammonium hydroxide gave **M4** in 80% yield.

The structures of intermediates and monomers (**M1**, **M2** and **M4**) were confirmed by NMR, FT-IR spectroscopy and elemental analysis. MALDI-TOF MS and UV-vis spectroscopy were also carried out to characterise **M1**. In the aromatic region of the ^1H NMR spectrum of **M1**, there are two doublets of equal intensity at 8.73 and 8.61 ppm, which correspond to protons of the PDI unit. The presence of two doublet (7.83 and 7.61 ppm) and two multiplet (7.51–7.49 and 7.37–7.33 ppm) signals of equal intensity can be attributed to the two fluorene moieties attached to PDI unit. The disappearance of NH_2 protons from intermediate **4** and the slight shift in the chemical shift of perylene protons compared to perylene dianhydride, further confirm the structure. The aliphatic region of the ^1H NMR spectrum constitute the signals of the alkyl substituents on the fluorene moieties and the ratio between integrated intensities of aromatic and aliphatic regions of the spectrum is consistent with the proposed structure of **M1** (Fig. S1†). In ^{13}C NMR spectrum of **M1**, the C=O peaks of the PDI unit appear at 162.1 ppm. The presence of 17 signals in the down field region in the range of 152.4–119.4 ppm correspond to 44 different aromatic carbon atoms and the signals in the range of 54.6–13.1 ppm account for the different aliphatic carbon atoms of the alkyl chains attached to the fluorene moieties confirming the structure of **M1** (Fig. S2†).

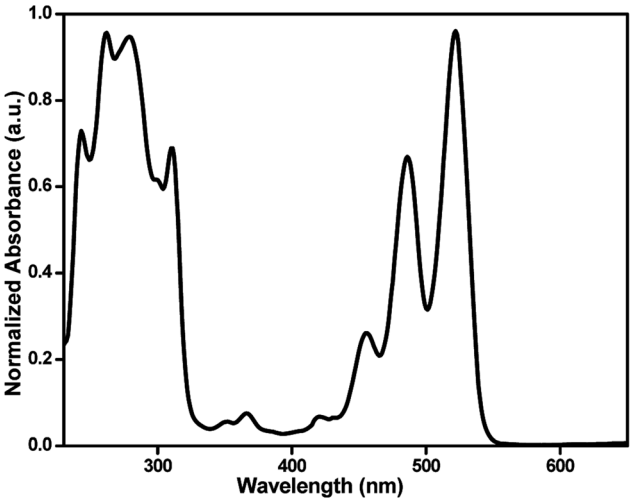

Fig. 1 Normalized absorbance spectrum of M1 in THF solution.

The FT-IR spectrum of **M1** clearly shows the presence of characteristic aromatic C–H stretching appearing at 2925 cm^{-1}, aliphatic C–H stretching appeared at 2852 cm^{-1}, O=CN stretching at 1705 and 1664 cm^{-1}, C=C stretching appeared at 1593 cm^{-1} and C–N stretching appeared at 1354 cm^{-1} and found similar as reported for other PDI derivatives.[46]

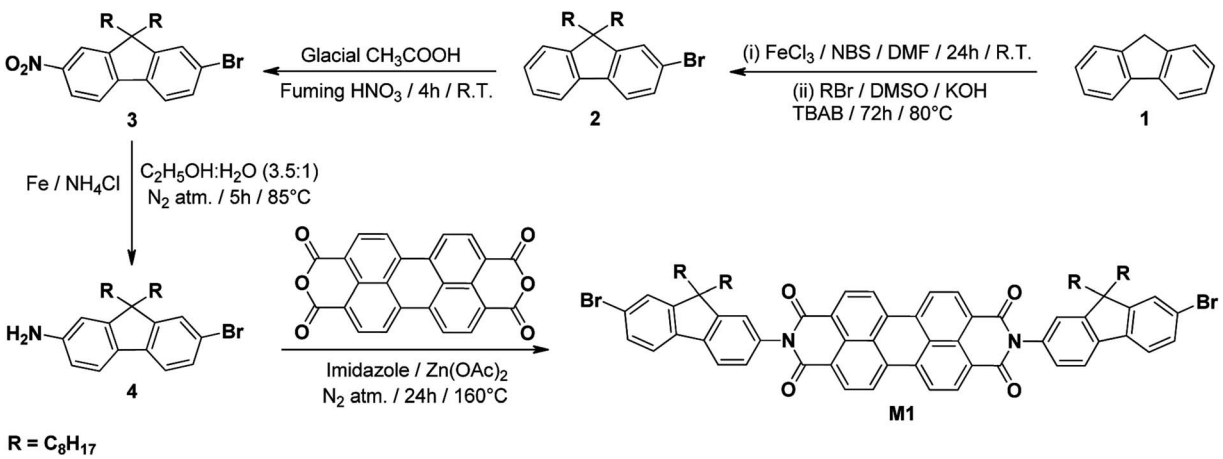

Scheme 1 Synthetic routes to design intermediates and monomer M1.

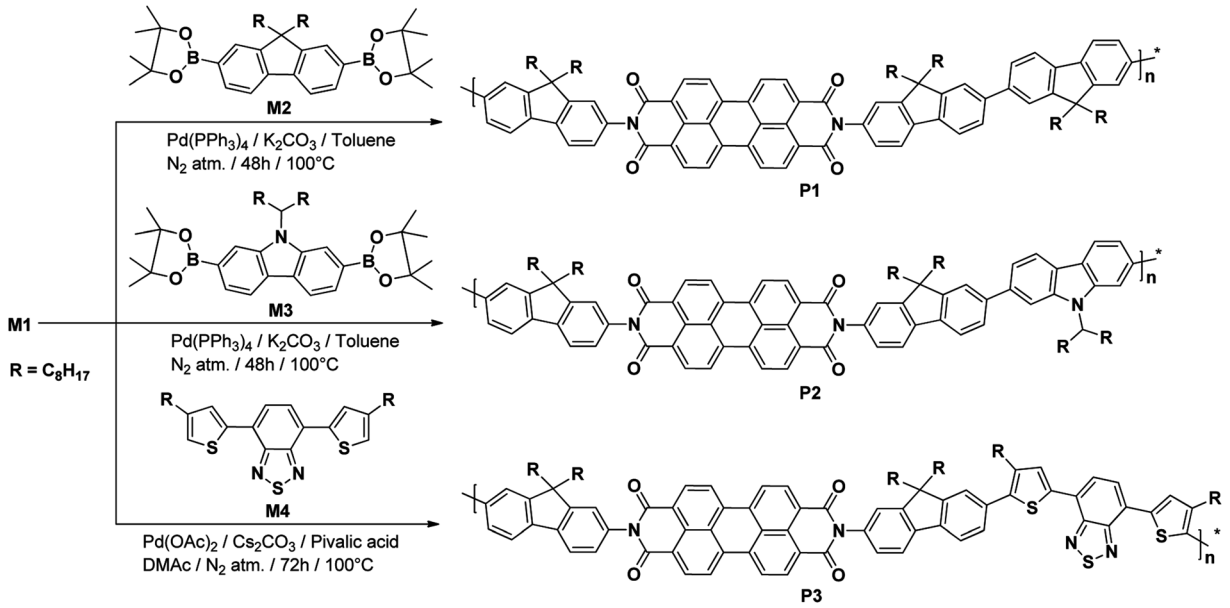

Scheme 2 Synthetic routes to design of polymers **P1–P3**.

Table 1 Molecular weights and thermal properties of polymers **P1–P3**

Polymers	M_w[a] (kg mol^{-1})	M_n[b] (kg mol^{-1})	PDI[c] (M_w/M_n)	T_5[d] (°C)
P1	14.77	9.66	1.53	381
P2	10.68	8.32	1.28	458
P3	16.02	12.42	1.29	380

[a] Weight-average molecular weight. [b] Number-average molecular weight. [c] Polydispersity index. [d] Onset decomposition temperature (5% weight loss).

The UV-vis spectrum of **M1** (Fig. 1) in THF, having three clearly distinguishable peaks in the region of 400–550 nm, which showed their absorption maxima at λ_{max} = 455, 485 and 520 nm consistent with the reported absorption spectra of PDI based monomers.[47] The above peaks are found match with different vibrational modes (2 ← 0, 1 ← 0 and 0 ← 0, respectively) combined with the PDI main transition dipole moment,[48] which is lined up along the long axis of the molecule. The more direct and supporting evidence for **M1** was obtained from the MALDI-TOF MS spectrum shown in Fig. S3,† where it can be seen that the experimental mass agrees well with the calculated mass.

The ^{1}H and ^{13}C NMR spectra of **M2** and **M4** are shown in Fig. S4–S7† and found to be in agreement with reported literature although in this work, **M2** and **M4** were synthesized by modified procedures with improved yield.[43,44]

N-substituted PDI based polymers **P1** and **P2** were synthesized by using Suzuki polymerization[49] whereas **P3** was synthesized by direct arylation polymerization.[50] Their synthetic routes are outlined in Scheme 2. The Suzuki polycondensation reaction of **M1** with **M2** or **M3** in the presence of $Pd(PPh_3)_4$, potassium carbonate and Aliquat 336 in mixture of toluene-water at 100 °C under N_2 atmosphere resulted in **P1** (81%

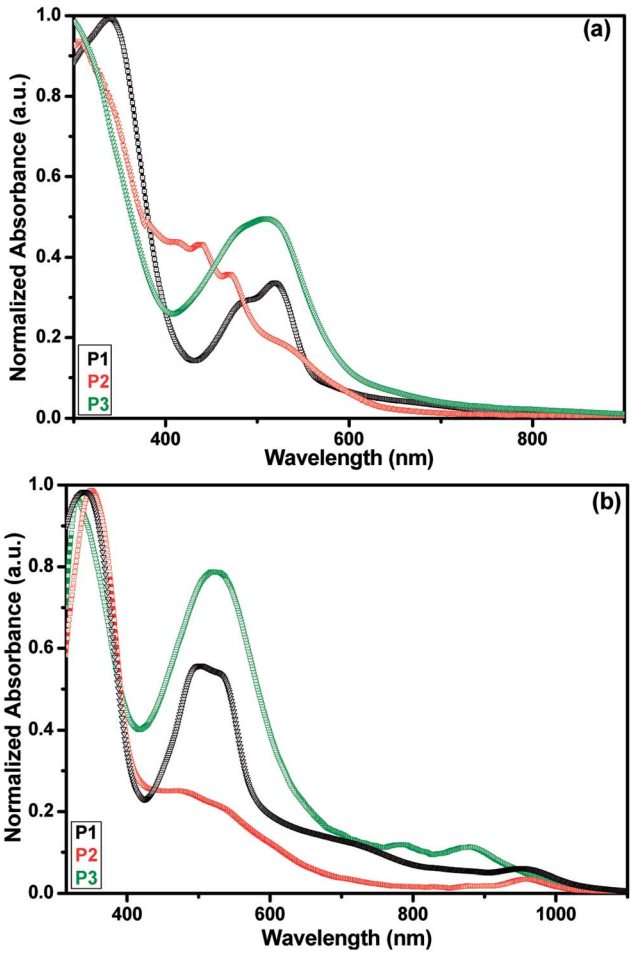

Fig. 2 Normalized absorbance spectra of **P1**, **P2** and **P3** (a) in THF solution and (b) films.

Table 2 Optical and electrochemical properties of polymers P1–P3

	λ_{max}[a] (nm)			Energy levels (eV)	
Polymers	Solution	Film	E_g^{opt} (eV)[b] (λ_{edge}/nm)[c]	E_{HOMO}[d]	E_{LUMO}[e]
P1	339, 519	341, 502, 951	2.08 (597)	−5.66	−3.58
P2	352, 520	354, 516, 954	1.80 (688)	−5.37	−3.57
P3	300, 510	329, 520, 784, 878	1.88 (660)	−5.50	−3.62

[a] UV-vis absorption maxima in THF solution and film. [b] Optical band gap $E_g^{opt} = 1240/\lambda_{edge}$. [c] Onset of thin films absorption spectra. [d] Calculated by equation HOMO = E_g^{opt} + LUMO (eV). [e] Calculated from the onset reduction potential.

yield) and **P2** (77% yield) respectively, whereas **P3** was synthesized by direct arylation polymerization of **M1** with **M4** in presence of pivalic acid, palladium acetate and caesium carbonate using *N*,*N*-dimethylacetamide at 100 °C under N_2 atmosphere in 80% yield. The purifications of the synthesized polymers were carried out by precipitation in cold CH_3OH than after Soxhlet extractions and finally reprecipitation from CH_3OH.

The polymeric structures of **P1–P3** were confirmed with ^{1}H NMR and FT-IR spectroscopy and their ^{1}H NMR spectra are shown in Fig. S8–S10.† In ^{1}H NMR spectra of **P1–P3**, the peaks at 8.63–7.29 ppm correspond to the aromatic protons whereas the peaks at 2.62–1.15 ppm can be attributed to CH_2 groups of alkyl chain. The signals in the range of 0.83–0.76 ppm arise from terminal CH_3 of alkyl substituent. The ^{1}H NMR spectrum of **P2** showed a singlet at 4.69 ppm confirming the presence of carbazole moiety in the polymeric chain. In **P3**, the signal at 7.18 ppm corresponds to aromatic protons of the benzothiadiazole moiety and at 2.62 ppm to the CH_2 protons directly attached to thiophene units. The measured proton intensities agree well with the structures of **P1–P3**.

The molecular weights and dispersities of **P1–P3** were determined by GPC against monodisperse polystyrene standards with THF as the eluent using the totalchrom software and their results are summarized in Table 1. The GPC measurements indicate that these polymers have weight-averaged molecular weights (M_w) of 14.77, 10.68 and 16.02 kg mol^{-1} with a narrow PDI of 1.53, 1.28 and 1.29 for **P1**, **P2** and **P3**, respectively. The thermogravimetric analysis (TGA) and differential scanning colorimetry (DSC) studies were performed to determine the thermal properties of the polymers **P1–P3** (Table 1). DSC curves of polymers reveal that no transitions were observed during the heating and cooling cycles whereas TGA analysis shows the onset decomposition temperature (T_5) higher than 380 °C at 5% weight loss. This suggested that the thermal stability of the polymers is sufficient for application in OSCs. The TGA graphs of the polymers are shown in Fig. S11.† The polymers **P1–P3** are found to be soluble in chlorinated solvents as well as in toluene and THF.

Optical properties

The UV-visible absorption spectroscopy was performed in THF solution and thin film to understand the optical properties of polymers **P1–P3**. Fig. 2 shows the absorption spectra of all polymers whereas their related data are given in Table 2. The polymers **P1–P3** (Fig. 2a) exhibited their absorption maxima in the range of 300 to 520 nm in THF solution. In these ranges, two clearly defined absorption bands were noticed, the first between 300 to 352 nm and the second in the range of 510 to 520 nm. These absorption bands located at lower wavelength can be assigned to π–π* transitions from the conjugated backbones localized on the donor or acceptor, whereas the higher wavelength absorption band can be assigned to intramolecular charge transfer (ICT) transitions inherent to the D–A system.[51] While comparing to film spectra with solution, the absorption maxima were red shifted with broadened area owing to strong inter-chain interaction and π–π stacking in the solid state which are beneficial for charge transport.[52] The solution and film spectra of polymers have almost the same absorption maxima in the range of 502 to 520 nm and are very close to the monomer **M1** due to the presence of the same PDI unit in all the polymers. Such close values in absorption maxima in monomer and polymers were also reported in other PDI based polymers.[53,54] The absorption spectra of the three polymers in film (Fig. 2b) showed absorption maxima at near infrared (NIR) region, 951 nm for **P1**, 954 nm for **P2** and 784 nm with a shoulder at 878 nm for **P3**. These absorptions at NIR region are relatively broad and weak in the range of 750 to 1000 nm and can be attributed to ICT between D–A units and simultaneously can increase the number of photons absorbed under solar radiation. The use of an OPV material that absorbs light in the NIR region and even above 1000 nm could increase the efficiency of devices in OSC applications.[55] In the film spectrum, the absorption maximum at 520 nm of **P3** was found to be slightly red shifted by *ca*. 10 nm as compared to solution indicating good intermolecular ordering in the solid state.[56] The optical band gaps (E_g^{opt}) of all the polymers were estimated from λ_{edge} of the thin film absorption spectra and found to be in the range of 1.80–2.08 eV. The absorption intensity and optical band gap value of **P3** are observed to be higher than those of **P2** which may be due to the incorporation of carbazole unit into the polymer backbone of **P2** leading to enhanced conjugation.[57] Further the presence of bulky octyl substituents in the thiophene units probably twist atom induce the main chain of **P3** leading to decrease coplanarity and intramolecular conjugation in solid state of the polymer.[58] All the polymers displayed comparable optical band gap values with literature values as reported for N-substituted PDI based alternating copolymers containing thiophene (2.0 eV),[36] oligothiophene (1.63–1.97 eV)[59] and phenylenevinylene (1.66 eV) units.[32] The narrower band

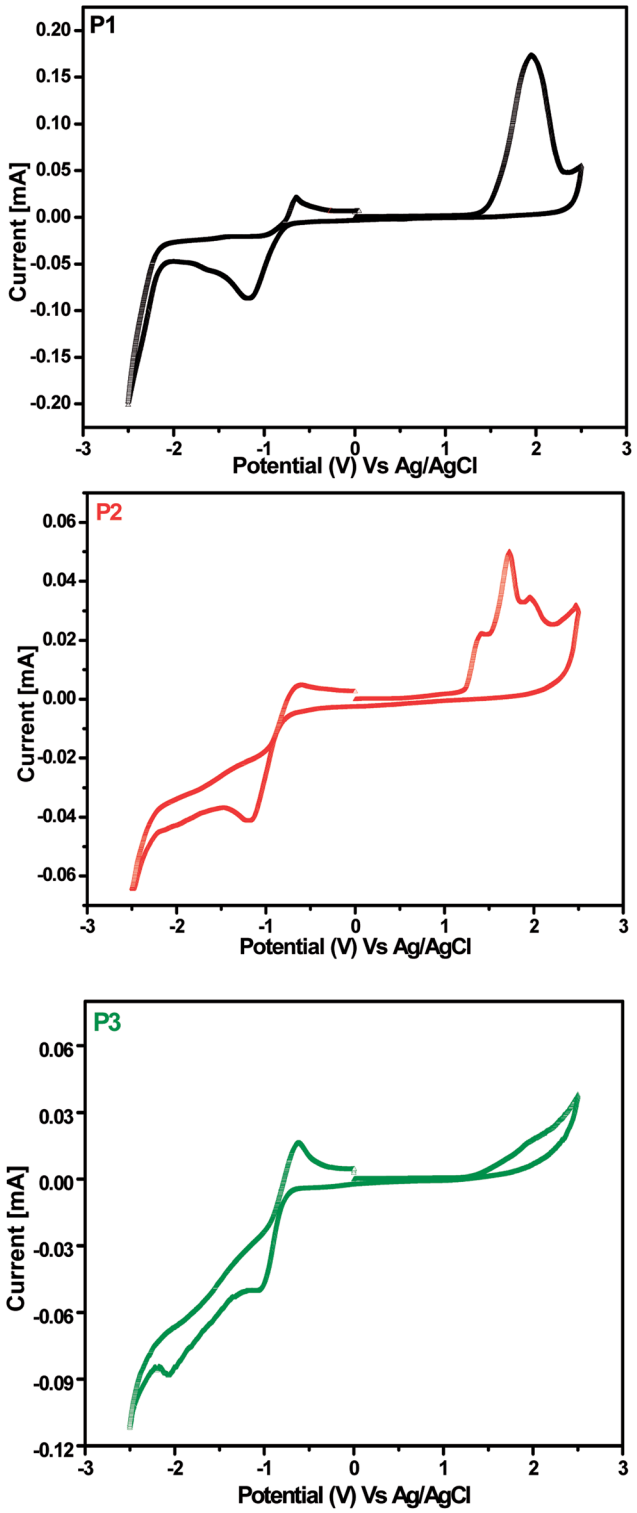

Fig. 3 Cyclic voltammetry curves of polymers P1–P3.

gaps of **P1–P3** can be assigned to well organised and planar structure of the conjugated polymers.

Electrochemical properties

The cyclic voltammetry (CV) studied were carried out to investigate the electrochemical properties of the polymers **P1–P3** using films on a glassy carbon working electrode (made by drop casting of their concentrated solution in $CHCl_3$) in CH_3CN solution having $[^nBu_4N]^+[ClO_4]^-$ (0.1 mol L^{-1}) as electrolyte at a scan rate of 50 mV s^{-1}. The voltammograms are shown in Fig. 3 and the results are summarized in Table 2. The highest occupied molecular orbital (HOMO) and lowest unoccupied molecular orbital (LUMO) energy levels were calculated by combining both absorption spectroscopy and CV. The LUMO energy levels were calculated from the first reduction onset potential using as reported equation $E_{LUMO} = -e\,(E_{red} + 4.4)$ eV and the HOMO energy levels were determined by E_g^{opt} plus LUMO energy levels.[60]

As displayed in Fig. 3, all the polymers show one or two reversible or quasi-reversible reduction and oxidation waves. The HOMO energy levels were calculated to be in the range of −5.37 to −5.66 eV for **P1–P3**, which are in remarkably good compliance with the ideal range of HOMO energy levels for achieving high air stability and high open-circuit voltage (V_{oc}) in OSCs.[61] In comparison to the HOMO energy level of **P3** (−5.50 eV), **P1** and **P2** (−5.66 and −5.37 eV, respectively) exhibit high lying and low lying HOMO energy levels by *ca.* 0.16 eV and 0.13 eV, respectively. The LUMO energy levels were calculated as −3.58 eV for **P1**, −3.57 eV for **P2** and −3.62 eV for **P3**. The LUMO energy levels of **P1** and **P2** are almost comparable whereas **P3** has slightly high lying LUMO energy level which can be due to the combined effect of two thiophene and one benzothiadiazole units. The HOMO and LUMO energy levels of **P1–P3** are found to be comparable with that of alternating phenylenevinylene polymer with PDI unit (HOMO and LUMO energy levels at −5.75 and −3.95 eV, respectively), which has shown one of the highest efficiency (PCE upto 2.32%) reported for N-substituted PDI based polymers.[32] The comparable LUMO energy level values of **P1–P3** illustrate that they can be used as n-type materials in OSCs.

Organic solar cell applications

BHJ solar cell devices were fabricated by blending the polymers **P1–P3** and P3HT with the device configuration of ITO/PEDOT:PSS/polymer:P3HT/Al and a pixel area of 0.04 cm^2 (for detail, see device fabrication) where PEDOT:PSS was used to modify the ITO electrode and to act as a hole-transporting layer. P3HT was used as the donor and N-substituted PDI based polymers **P1–P3** as the acceptor to design the photoactive layers. DCB was used as a processing solvent since it was reported to afford the perfect quality of blended films.[62] The OSC device performance was optimized in three different binary compositions of **P1**/**P2**/**P3**:P3HT weight ratios *i.e.* 1 : 1, 1.5 : 1 and 2 : 1 to achieve best PCE. The current density *versus* voltage (*J*–*V*) curves of the OSCs fabricated with the optimized D : A ratio are shown in Fig. 4 and their corresponding open-circuit voltage (V_{oc}), short-circuit current (J_{sc}), fill factor (FF) and PCE are listed in Table 3. The photovoltaic performances of PSCs are greatly influenced by film morphology of **P1–P3** and P3HT since the data from photovoltaic studies reveal that the 1 : 1 weight ratio of **P1**/**P2**/**P3**:P3HT blends exhibit higher PCEs (0.82%, 1.22% and 1.96%, respectively) in comparison to other weight ratios *i.e.* 1.5 : 1 and 2 : 1 blends (PCEs ranges from 0.23 to 1.11%),

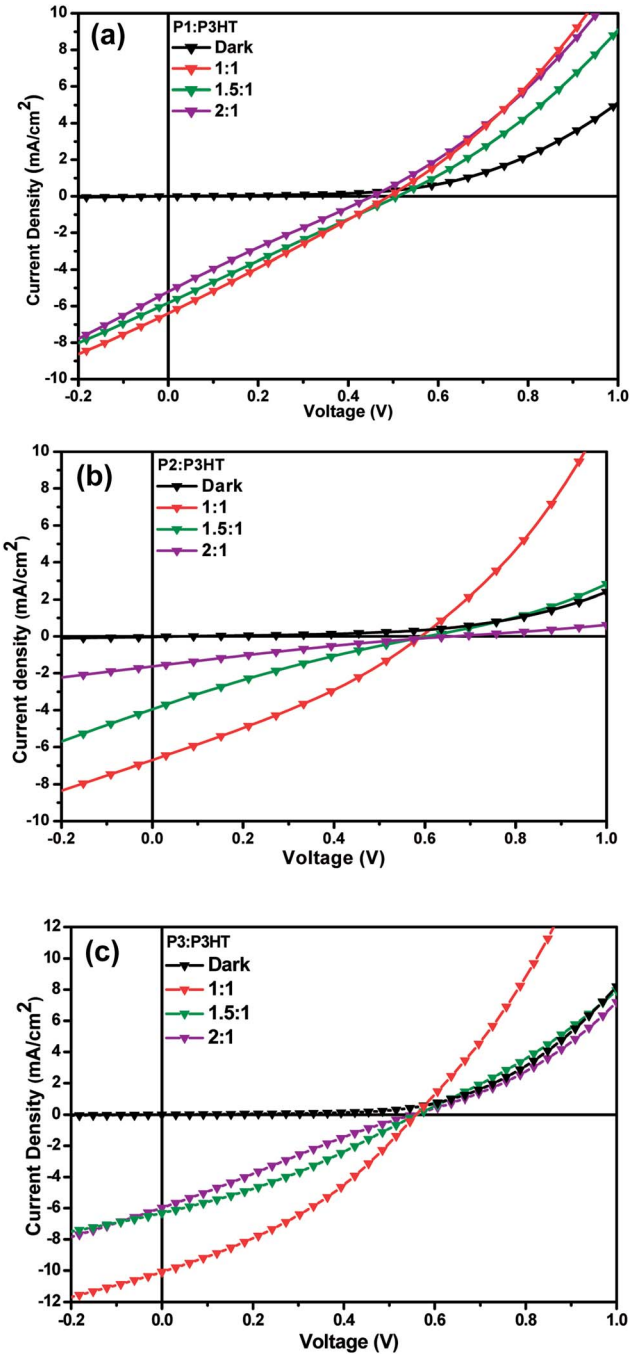

Fig. 4 *J*–*V* curves of the OSCs based on (a) **P1**:P3HT and (b) **P2**:P3HT and (c) **P3**:P3HT.

suggesting a further increase of polymer content and decrease of P3HT content in the photoactive layer had an unfavourable impact on both J_{sc} and FF resulting in an overall decrease in PCE. The high polymer and low P3HT content in blend films probably attributed to the improper thickness of photo-active layer leading to higher current leakage, which in turn account for the poor photovoltaic performances observed in devices. The relatively better performance of 1 : 1 **P1**/**P2**/**P3**:P3HT blends can be due to more favourable film morphology and proper thickness of the active layers with smoothened surface having

Table 3 Photovoltaic properties of polymers **P1**–**P3**

Polymers	Ratio Polymer : P3HT	J_{sc} (mA cm^{-2})	V_{oc} (V)	FF (%)	PCE (%)	Roughness (rms)
P1	1 : 1	6.43	0.49	25.83	0.82	1.79
P1	1.5 : 1	5.82	0.51	24.79	0.74	2.34
P1	2 : 1	5.21	0.45	24.03	0.57	2.85
P2	1 : 1	6.70	0.59	30.81	1.22	1.67
P2	1.5 : 1	3.94	0.60	21.26	0.51	2.43
P2	2 : 1	1.62	0.66	21.41	0.23	2.90
P3	1 : 1	10.12	0.55	34.63	1.96	0.65
P3	1.5 : 1	6.32	0.56	31.22	1.11	1.44
P3	2 : 1	5.98	0.55	24.21	0.80	2.66

lower rms values (1.79, 1.67 and 0.65 nm, respectively). The PCE for the binary 1 : 1 film of **P3**:P3HT blend device reached upto 1.96% (highest among all devices in all tested ratios) with V_{oc} of 0.55 V, J_{sc} of 10.12 mA cm^{-2} and a FF of 34.63%. In comparison, **P1**:P3HT/**P2**:P3HT devices (for ratio 1 : 1) showed PCEs of 1.22/0.82%, V_{oc} of 0.59/0.49 V, J_{sc} of 6.70/6.43 mAcm^{-2} and FF of 25.83/30.81%, respectively. The higher efficiency obtained with **P3** based device can be attributed to higher J_{sc} and FF owing to better conjugation and broader absorption spectrum of polymer. J_{sc} ideally correlates with the energetic difference between HOMO–LUMO energy levels of D–A segments of blend films and consequently relates to the exciton dissociation. Comparing OPV devices constructed with 1 : 1 weight ratio, **P3** blend shows a higher J_{sc} of 10.12 mA cm^{-2} relative to **P1** and **P2** (J_{sc} of 6.70 and 6.43 mA cm^{-2}, respectively) analogues and hence higher value of exciton dissociation which could be the reason for higher PCE in **P3** based OSC. However in the present study, the V_{oc},J_{sc}, FF and PCE show a linear trend with all the tested weight ratios of **P1**/**P2**/**P3**:P3HT blend films, since these photovoltaic device properties are influenced by other features such as molecular structure, charge transport and the surface morphology of the blended films as well. Even though the device performances of the N-substituted PDI based polymers were low, these are comparable to some of the previously reported for the BHJ photovoltaic devices based on a blend of tris(thienylenevinylene)-substituted polythiophene and poly [perylene diimide-*alt*-bis(dithienothiophene)].[63] The PCEs of these devices are less than that reported for blend device of alternating phenylenevinylene copolymer with PDI unit and a poly(3-phenylhydrazonethiophene) donor, which resulted a PCE of 2.32%. The improvement was attributed to thermal annealing of the blend film which initiate the fine mixing morphology of two components and the higher hole mobility in the films.[32] However, the lower PCE in our devices in comparison to the above reported device efficiency is primarily restricted by the low values of V_{oc} and FF. The low values of FF of our devices can be attributed to the electron traps present in polymer phase which contributes to the recombination losses. The high FF values of the solar cell devices can be achieved by better fabrication or design with proper selection of device engineering strategies,[64,65] improving morphology of

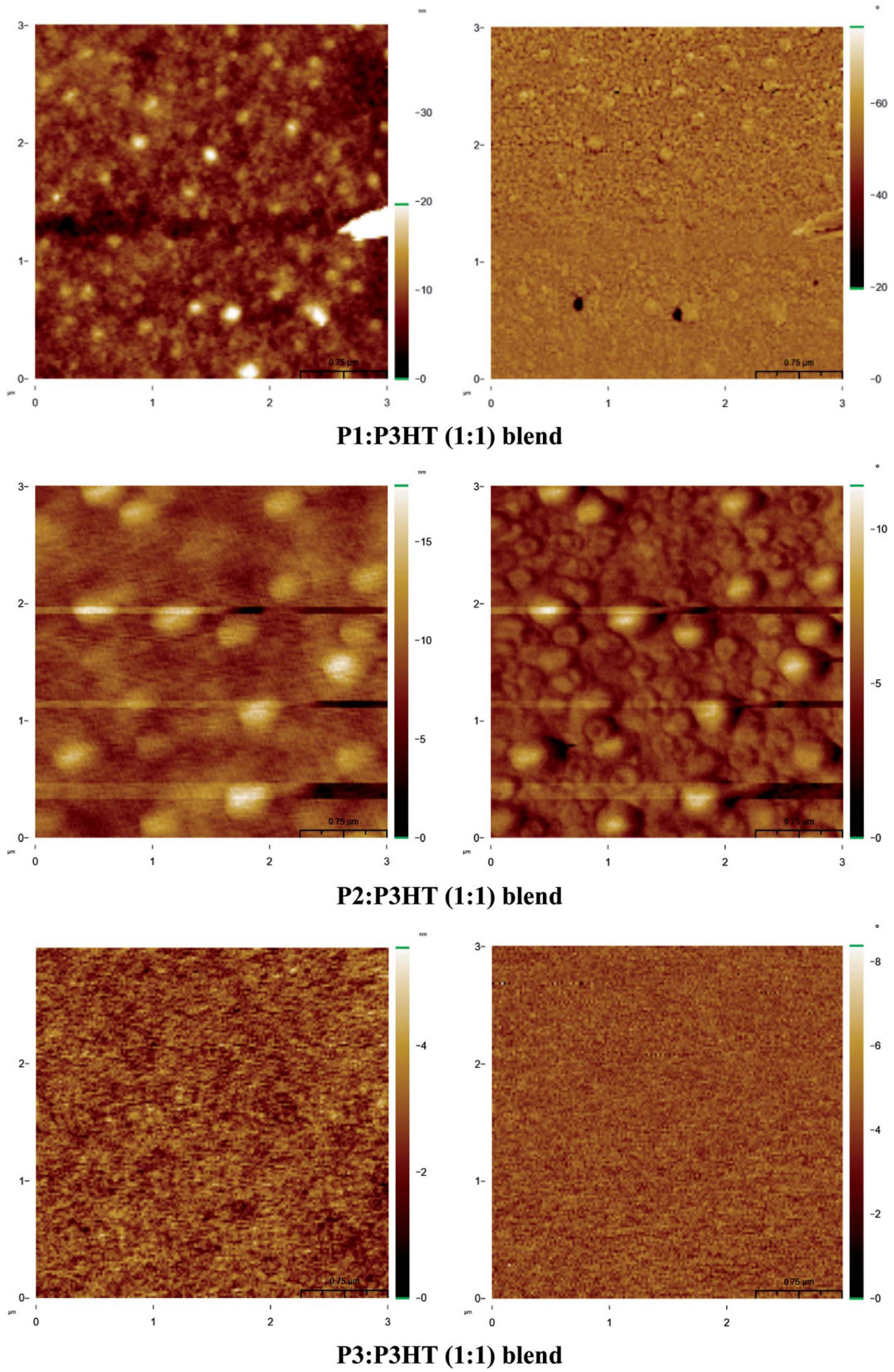

Fig. 5 AFM topographic (left) and phase (right) images of **P1**/**P2**/**P3**:P3HT blend films.

photoactive layer with controlled thermal treatment[66] and proper selection of processing additives.[67] It was reported that additives are useful to enhance the miscibility between two components of the photoactive layer and found necessary for optimizing photovoltaic device performances by increasing FF.[68] The PCEs obtained for N-substituted PDI based polymers are limited of their application in OSCs due to reduced exciton dissociation efficiency and/or increased charge recombination. Therefore, further experiments are in progress to improve the photocurrent for OSCs to achieve better PCE by modifying the structure as well as improving the surface morphology of the blend films.

Morphological studies

The surface morphology of the photoactive layer in the BHJ solar cells was found to be an important aspect to control the charge carrier transport into blend films and impact on the performance of OSCs.[69] To further understand the different photovoltaic performance of PSCs based on **P1**/**P2**/**P3**:P3HT blend films, atomic force microscopy (AFM) studies were carried out to investigate the morphology of the active layers using tapping mode. Fig. 5 shows topographic images and phase images for **P1**:P3HT, **P2**:P3HT and **P3**:P3HT blend films in DCB solution for 1 : 1 weight ratio whereas other topographic images and phase images for remaining 1.5 : 1 and 2 : 1 weight ratios are given in Fig. S12.† The root-mean-square (rms) roughnesses of these films measured from topographic images are in range of 0.65 to 2.90 nm. In all AFM images, we observed a phase-separated interpenetrating network with sizable P3HT domains. Some of phase-separation are important and necessary for systematic formation of free carriers to generate optimal photovoltaic properties of PSCs.[70] The phase images of **P1**:P3HT, **P2**:P3HT and **P3**:P3HT blend films in the ratio of 1 : 1 are quite different (rms roughness 1.79, 1.67 and 0.65 nm, respectively) and revealed that the P3HT domains in the **P3**:P3HT blend film were smaller than those in the **P1**:P3HT and **P2**:P3HT blend films, indicating better compatibility between the P3HT and polymer in case of **P3**. This can be attributed to the high solubility and feasible solution processability of thiophene–benzothiadiazole–thiophene[71] containing polymer **P3** which may allow easier incorporation of P3HT into polymer matrix. Among all blend films, more uniform morphology (rms 0.65 nm) with lower defect density and larger aggregation domains was observed for **P3**:P3HT blend film in 1 : 1 ratio, which is favourable to electron transport leading to the highest PCE 1.96% with highest FF value (34.63%). However, the **P1**/**P2**/**P3**:P3HT blend films in the ratio of 1 : 1 each showed more intermixed, smooth and homogeneous morphology in comparison to 1.5 : 1 and 2 : 1 blend films. The blend films with weight ratios of 1.5 : 1 and 2 : 1 show higher rms values ranges from 1.44 to 2.43 nm and ranges from 2.66 to 2.90 nm, respectively and therefore exhibit larger domain size resulting in ineffective exciton dissociation and lower PCE. The phase images (Fig. S12†) of **P1**/**P2**/**P3**:P3HT blend films having weight ratios of 1.5 : 1 and 2 : 1 also support the above assertion. However, the distribution of P3HT units in the polymer for **P1**/**P2**/**P3**:P3HT blend films was less uniform for 1.5 : 1 and 2 : 1 ratio as the polymer content is increased (weight% of polymer are 60% and 66.67%, respectively) and in respect of polymer the P3HT content decreased (weight% of P3HT are 40% and 33.33%, respectively), the films became more coarser owing to poor solubility, high molecular stacking and electrostatic interactions resulting in self-aggregation of polymers with reduced compatibility with P3HT.[72] The 1 : 1 blend ratio of **P1**:P3HT, **P2**:P3HT and **P3**:P3HT gave optimal morphology in films for charge transport and correlates well with the observed device performances and their data are summarized in Table 3.

Conclusions

In the present work, an efficient and facile route was developed to synthesize the new N-substituted PDI based monomer **M1**. Three novel N-substituted PDI based low band gap polymers **P1**, **P2** and **P3** were synthesized by using palladium catalysed polycondensation reactions for organic solar cell applications. The structures of **M1** and the newly designed polymers were confirmed by NMR, FT-IR and UV-vis spectroscopy. Polymers were further characterized by CV and GPC. The polymers exhibit good solubility in common organic solvents and thermal stability with T_5 higher than 380 °C at 5% weight loss. The absorption spectra of **P1–P3** were broad and extended up to about 954 nm in to the NIR region with shorter wavelength maxima in the range of 502 to 520 nm and E_g^{opt} in the range of 1.80–2.08 eV. GPC studies revealed that all the polymers have good molecular weight (M_w) ranging from 10.68 to 16.02 kg mol^{-1}. From cyclic voltammetric studies, it was found that the HOMO energy levels ranged from −5.37 to −5.66 eV whereas the LUMO energy levels ranged from −3.57 to −3.62 eV. **P1**/**P2**/**P3**:P3HT based BHJs were fabricated in three different weight ratios *i.e.* 1 : 1, 1.5 : 1 and 2 : 1 by solution processing and it was found that the weight ratio of 1 : 1 for binary **P3**:P3HT blend is the most optimal system and showed a J_{sc} of 10.12 mA cm^{-2}, a V_{oc} of 0.55 V and FF of 34.63% with an PCE of 1.96% which is among the highest reported for PDI based BHJ solar cells. Further, the high polymer and low P3HT content in blend films adversely affect the film morphology of the photo-active layer resulting in charge recombination and current leakage owing to micro-phase separation and aggregation of polymer which in turn lead to low photovoltaic performances of PSCs based on 1.5 : 1 and 2 : 1 weight ratio.

Conflicts of interest

There are no conflicts of interest to declare.

Acknowledgements

The financial support obtained from Department of Science & Technology, India (DST project no. SB/S1/OC-12/2013) is highly appreciated by authors to complete this research. Authors are also thankful to DMSE, IIT Delhi for providing laboratory facilities, Central Research Facility (CRF) and Nanoscale Research Facility (NRF), IIT Delhi for necessary spectral studies.

S. M. acknowledges the University Grants Commission (UGC), India for providing Teacher Research Fellowship under Faculty Improvement program. T. M. gratefully acknowledges UGC for a Maulana Azad National Fellowship.

Notes and references

1 L. Lu, T. Zheng, Q. Wu, A. M. Schneider, D. Zhao and L. Yu, Recent Advances in Bulk Heterojunction Polymer Solar Cells, *Chem. Rev.*, 2015, **115**, 12666–12731.

2 Y. Lin, Y. Li and X. Zhan, Small molecule semiconductors for high-efficiency organic photovoltaics, *Chem. Soc. Rev.*, 2012, **41**, 4245–4272.

3 R. Ganesamoorthy, G. Sathiyan and P. Sakthivel, Review: Fullerene based acceptors for efficient bulk heterojunction organic solar cell applications, *Sol. Energy Mater. Sol. Cells*, 2017, **161**, 102–148.

4 P. Sonar, J. P. Fong Lim and K. L. Chan, Organic non-fullerene acceptors for organic photovoltaics, *Energy Environ. Sci.*, 2011, **4**, 1558–1574.

5 L. Chen and W. Henrike, Perylene Imides for Organic Photovoltaics: Yesterday, Today, and Tomorrow, *Adv. Mater.*, 2012, **24**, 613–636.

6 M. A. Alamoudi, J. I. Khan, Y. Firdaus, K. Wang, D. Andrienko, P. M. Beaujuge and F. Laquai, Impact of Nonfullerene Acceptor Core Structure on the Photophysics and Efficiency of Polymer Solar Cells, *ACS Energy Lett.*, 2018, 802–811.

7 D. Sun, D. Meng, Y. Cai, B. Fan, Y. Li, W. Jiang, L. Huo, Y. Sun and Z. Wang, Non-Fullerene-Acceptor-Based Bulk-Heterojunction Organic Solar Cells with Efficiency over 7%, *J. Am. Chem. Soc.*, 2015, **137**, 11156–11162.

8 F. Yang, X. Wang, G. Feng, J. Ma, C. Li, J. Li, W. Ma and W. Li, A new strategy for designing polymer electron acceptors: electronrich conjugated backbone with electron-deficient side units, *Sci. China: Chem.*, 2018, **61**, 824–829.

9 N. Liang, W. Jiang, J. Hou and Z. Wang, New developments in non-fullerene small molecule acceptors for polymer solar cells, *Mater. Chem. Front.*, 2017, **1**, 1291–1303.

10 Y.-J. Hwang, H. Li, B. A. E. Courtright, S. Subramaniyan and S. A. Jenekhe, Nonfullerene Polymer Solar Cells with 8.5% Efficiency Enabled by a New Highly Twisted Electron Acceptor Dimer, *Adv. Mater.*, 2016, **28**, 124–131.

11 Y. Lin, Q. He, F. Zhao, L. Huo, J. Mai, X. Lu, C.-J. Su, T. Li, J. Wang, J. Zhu, Y. Sun, C. Wang and X. Zhan, A Facile Planar Fused-Ring Electron Acceptor for As-Cast Polymer Solar Cells with 8.71% Efficiency, *J. Am. Chem. Soc.*, 2016, **138**, 2973–2976.

12 H. Zhong, C.-H. Wu, C.-Z. Li, J. Carpenter, C.-C. Chueh, J.-Y. Chen, H. Ade and A. K. Y. Jen, Rigidifying Nonplanar Perylene Diimides by Ring Fusion Toward Geometry-Tunable Acceptors for High-Performance Fullerene-Free Solar Cells, *Adv. Mater.*, 2016, **28**, 951–958.

13 L. Cheng, Y. Changshi, L. Wenbin, L. Shijie, J. Xudong, F. Guitao, Z. Jianqi, X. Yunhua and L. Weiwei, Multifunctional Diketopyrrolopyrrole-Based Conjugated Polymers with Perylene Bisimide Side Chains, *Macromol. Rapid Commun.*, 2018, **39**, 1700611.

14 X. Zhan, A. Facchetti, S. Barlow, T. J. Marks, M. A. Ratner, M. R. Wasielewski and S. R. Marder, Rylene and Related Diimides for Organic Electronics, *Adv. Mater.*, 2011, **23**, 268–284.

15 N. I. Georgiev, A. R. Sakr and V. B. Bojinov, Design and synthesis of novel fluorescence sensing perylene diimides based on photoinduced electron transfer, *Dyes Pigm.*, 2011, **91**, 332–339.

16 H.-Y. Tsai and K.-Y. Chen, Synthesis and optical properties of novel asymmetric perylene bisimides, *J. Lumin.*, 2014, **149**, 103–111.

17 L. Ye, K. Sun, W. Jiang, S. Zhang, W. Zhao, H. Yao, Z. Wang and J. Hou, Enhanced Efficiency in Fullerene-Free Polymer Solar Cell by Incorporating Fine-designed Donor and Acceptor Materials, *ACS Appl. Mater. Interfaces*, 2015, **7**, 9274–9280.

18 E. Kozma, W. Mróz and F. Galeotti, A polystyrene bearing perylene diimide pendants with enhanced solid state emission for white hybrid light-emitting diodes, *Dyes Pigm.*, 2015, **114**, 138–143.

19 Y. Huang, L. Fu, W. Zou, F. Zhang and Z. Wei, Ammonia Sensory Properties Based on Single-Crystalline Micro/Nanostructures of Perylenediimide Derivatives: Core-Substituted Effect, *J. Phys. Chem. C*, 2011, **115**, 10399–10404.

20 S. Vasimalla, N. V. V. Subbarao, M. Gedda, D. K. Goswami and P. K. Iyer, Effects of Dielectric Material, HMDS Layer, and Channel Length on the Performance of the Perylenediimide-Based Organic Field-Effect Transistors, *ACS Omega*, 2017, **2**, 2552–2560.

21 F. Wurthner and M. Stolte, Naphthalene and perylene diimides for organic transistors, *Chem. Commun.*, 2011, **47**, 5109–5115.

22 L. Flamigni, B. Ventura, C.-C. You, C. Hippius and F. Würthner, Photophysical Characterization of a Light-Harvesting Tetra Naphthalene Imide/Perylene Bisimide Array, *J. Phys. Chem. C*, 2007, **111**, 622–630.

23 T. M. Wilson, M. J. Tauber and M. R. Wasielewski, Toward an n-Type Molecular Wire: Electron Hopping within Linearly Linked Perylenediimide Oligomers, *J. Am. Chem. Soc.*, 2009, **131**, 8952–8957.

24 W. Ma, L. Qin, Y. Gao, W. Zhang, Z. Xie, B. Yang, L. Liu and Y. Ma, A perylene bisimide network for high-performance n-type electrochromism, *Chem. Commun.*, 2016, **52**, 13600–13603.

25 R. Xin, J. Feng, C. Zeng, W. Jiang, L. Zhang, D. Meng, Z. Ren, Z. Wang and S. Yan, Nonfullerene-Acceptor All-Small-Molecule Organic Solar Cells Based on Highly Twisted Perylene Bisimide with an Efficiency of over 6%, *ACS Appl. Mater. Interfaces*, 2017, **9**, 2739–2746.

26 E. Kozma and M. Catellani, Perylene diimides based materials for organic solar cells, *Dyes Pigm.*, 2013, **98**, 160–179.

27 Y. Kim and E. Lim, Development of Polymer Acceptors for Organic Photovoltaic Cells, *Polymers*, 2014, **6**, 382–407.

28 Y. Avlasevich, C. Li and K. Mullen, Synthesis and applications of core-enlarged perylene dyes, *J. Mater. Chem.*, 2010, **20**, 3814–3826.

29 Y. Li, L. Tan, Z. Wang, H. Qian, Y. Shi and W. Hu, Air-Stable n-Type Semiconductor: Core-Perfluoroalkylated Perylene Bisimides, *Org. Lett.*, 2008, **10**, 529–532.

30 J. L. Segura, H. Herrera and P. Bauerle, Oligothiophene-functionalized naphthalimides and perylene imides: design, synthesis and applications, *J. Mater. Chem.*, 2012, **22**, 8717–8733.

31 E. E. Neuteboom, S. C. J. Meskers, P. A. van Hal, J. K. J. van Duren, E. W. Meijer, R. A. J. Janssen, H. Dupin, G. Pourtois, J. Cornil, R. Lazzaroni, J.-L. Brédas and D. Beljonne, Alternating Oligo(p-phenylene vinylene)−Perylene Bisimide Copolymers: Synthesis, Photophysics, and Photovoltaic Properties of a New Class of Donor−Acceptor Materials, *J. Am. Chem. Soc.*, 2003, **125**, 8625–8638.

32 J. A. Mikroyannidis, M. M. Stylianakis, G. D. Sharma, P. Balraju and M. S. Roy, A Novel Alternating Phenylenevinylene Copolymer with Perylene Bisimide Units: Synthesis, Photophysical, Electrochemical, and Photovoltaic Properties, *J. Phys. Chem. C*, 2009, **113**, 7904–7912.

33 Z. Liang, R. A. Cormier, A. M. Nardes and B. A. Gregg, Developing perylene diimide based acceptor polymers for organic photovoltaics, *Synth. Met.*, 2011, **161**, 1014–1021.

34 W. Fu, C. He, S. Jiang, Z. Chen, J. Zhang, Z. Li, S. Yan and R. Zhang, Synthesis of a Polymeric Electron Acceptor Based on Perylenediimide-Bridged Ladder Polysiloxane, *Macromolecules*, 2011, **44**, 203–207.

35 S.-H. Jin, T. Ban, J. Park, Y.-S. Gal and J. Wook Lee, Synthesis and Photovoltaic Properties of Low-Band Gap Copolymers Containing Perylene Diimide Derivatives, *Mol. Cryst. Liq. Cryst.*, 2013, **578**, 95–103.

36 S. Koyuncu, M. Kus, S. Demic, İ. Kaya, E. Ozdemir and S. Icli, Electrochemical and optical properties of novel donor-acceptor thiophene-perylene-thiophene polymers, *J. Polym. Sci., Part A: Polym. Chem.*, 2008, **46**, 1974–1989.

37 X. Shiqing, K. Eun Hoo, W. Alexander and N. Ei-ichi, Pd- and Ni-catalyzed cross-coupling reactions in the synthesis of organic electronic materials, *Sci. Technol. Adv. Mater.*, 2014, **15**, 044201.

38 X. Zhang, Y. Gao, S. Li, X. Shi, Y. Geng and F. Wang, Synthesis of poly(5,6-difluoro-2,1,3-benzothiadiazole-alt-9,9-dioctyl-fluorene) via direct arylation polycondensation, *J. Polym. Sci., Part A: Polym. Chem.*, 2014, **52**, 2367–2374.

39 A. J. H. Brian, S. Furniss, P. W. G. Smith, A. R. Tatchell and R. Vogel's, *Textbook of Practical Organic Chemistry*, 5th edn, ELBS, Longman Group, London, 1989.

40 S. Meena, F. Alam, V. Dutta and J. Jacob, Synthesis and photovoltaic device studies of azo-linked low-bandgap polymers, *Polym. Int.*, 2017, **66**, 593–603.

41 M. Ghaemy and M. Barghamadi, Synthesis and characterization of novel photoactive polyamide derived from substituted fluorene by copper (I) catalyst, *J. Appl. Polym. Sci.*, 2009, **114**, 3464–3471.

42 S. J. Liu, Q. Zhao, R. F. Chen, Y. Deng, Q. L. Fan, F. Y. Li, L. H. Wang, C. H. Huang and W. Huang, π-Conjugated Chelating Polymers with Charged Iridium Complexes in the Backbones: Synthesis, Characterization, Energy Transfer, and Electrochemical Properties, *Chem. - Eur. J.*, 2006, **12**, 4351–4361.

43 R. Wang, C. Zhang, W. Wang and T. Liu, Preparation, morphology, and biolabeling of fluorescent nanoparticles based on conjugated polymers by emulsion polymerization, *J. Polym. Sci., Part A: Polym. Chem.*, 2010, **48**, 4867–4874.

44 J.-C. Li, S.-J. Kim, S.-H. Lee, Y.-S. Lee, K. Zong and S.-C. Yu, Synthesis and characterization of a thiophene-benzothiadiazole copolymer, *Macromol. Res.*, 2009, **17**, 356–360.

45 O. A. Kucherak, P. Didier, Y. Mély and A. S. Klymchenko, Fluorene Analogues of Prodan with Superior Fluorescence Brightness and Solvatochromism, *J. Phys. Chem. Lett.*, 2010, **1**, 616–620.

46 A. K. Maiti, R. Aroca and Y. Nagao, Spectroscopic characterization and Langmuir–Blodgett films of N,N-symmetrical dialkyl-3,4:9,10-perylenebis(dicarboximide)s, *J. Raman Spectrosc.*, 1993, **24**, 351–356.

47 M. J. Farooqi, M. A. Penick, J. Burch, G. R. Negrete and L. Brancaleon, Characterization of novel perylene diimides containing aromatic amino acid side chains, *Spectrochim. Acta, Part A*, 2016, **153**, 124–131.

48 I. A. Fedorov, Y. N. Zhuravlev and V. P. Berveno, Structural and electronic properties of perylene from first principles calculations, *J. Chem. Phys.*, 2013, **138**, 094509.

49 R.-D. Rusu and A. D. Schluter, Progress in the Suzuki polycondensation of fluorene monomers, *RSC Adv.*, 2014, **4**, 57026–57034.

50 J.-R. Pouliot, F. Grenier, J. T. Blaskovits, S. Beaupré and M. Leclerc, Direct (Hetero)arylation Polymerization: Simplicity for Conjugated Polymer Synthesis, *Chem. Rev.*, 2016, **116**, 14225–14274.

51 S. Baysec, N. Akbasoglu Unlu, S. O. Hacioglu, Y. Arslan Udum, A. Cirpan and L. Toppare, Electrochemical Properties of Perylene Diimide (PDI) and Benzotriazole (Btz) Bearing Conjugated Polymers to Investigate the Effect of π-Bridge on Electrochemical Properties, *J. Macromol. Sci., Part A: Pure Appl.Chem.*, 2015, **52**, 1–9, DOI: 10.1080/10601325.10602014.10976742.

52 C. Ramanan, C. H. Kim, T. J. Marks and M. R. Wasielewski, Excitation Energy Transfer within Covalent Tetrahedral Perylenediimide Tetramers and Their Intermolecular Aggregates, *J. Phys. Chem. C*, 2014, **118**, 16941–16950.

53 P. Yan, A. Chowdhury, M. W. Holman and D. M. Adams, Self-Organized Perylene Diimide Nanofibers, *J. Phys. Chem. B*, 2005, **109**, 724–730.

54 E. E. Neuteboom, S. C. J. Meskers, E. W. Meijer and R. A. J. Janssen, Photoluminescence of Self-organized Perylene Bisimide Polymers, *Macromol. Chem. Phys.*, 2004, **205**, 217–222.

55 L. Dou, Y. Liu, Z. Hong, G. Li and Y. Yang, Low-Bandgap Near-IR Conjugated Polymers/Molecules for Organic Electronics, *Chem. Rev.*, 2015, **115**, 12633–12665.

56 J. Roncali, Molecular Engineering of the Band Gap of π-Conjugated Systems: Facing Technological Applications, *Macromol. Rapid Commun.*, 2007, **28**, 1761–1775.

57 H.-J. Wang, J.-Y. Tzeng, C.-W. Chou, C.-Y. Huang, R.-H. Lee and R.-J. Jeng, Novel polythiophene derivatives functionalized with conjugated side-chain pendants comprising triphenylamine/carbazole moieties for photovoltaic cell applications, *Polym. Chem.*, 2013, **4**, 506–519.

58 T. Xu and L. Yu, How to design low bandgap polymers for highly efficient organic solar cells, *Mater. Today*, 2014, **17**, 11–15.

59 S. Chen, Y. Liu, W. Qiu, X. Sun, Y. Ma and D. Zhu, Oligothiophene-Functionalized Perylene Bisimide System: Synthesis, Characterization, and Electrochemical Polymerization Properties, *Chem. Mater.*, 2005, **17**, 2208–2215.

60 K. Nakabayashi, M. Yamada and H. Mori, Perylene bisimide-based semiconducting polymers: Synthesis via palladium-catalyzed direct arylation, characterization, optoelectrical properties, and nanomorphology, *J. Polym. Sci., Part A: Polym. Chem.*, 2016, **54**, 3151–3158.

61 *Primary Photoexcitation in Conjugated Polymers: Molecular Exciton vs. Semiconductor Band Model*, ed. N. S. Sariciftci, World Scientific, Singapore, 1997.

62 S. Dai, P. Cheng, Y. Lin, Y. Wang, L. Ma, Q. Ling and X. Zhan, Perylene and naphthalene diimide polymers for all-polymer solar cells: a comparative study of chemical copolymerization and physical blend, *Polym. Chem.*, 2015, **6**, 5254–5263.

63 Z. Tan, E. Zhou, X. Zhan, X. Wang, Y. Li, S. Barlow and S. R. Marder, Efficient all-polymer solar cells based on blend of tris(thienylenevinylene)-substituted polythiophene and poly[perylene diimide-alt-bis(dithienothiophene)], *Appl. Phys. Lett.*, 2008, **93**, 073309.

64 X. Guo, N. Zhou, S. J. Lou, J. Smith, D. B. Tice, J. W. Hennek, R. P. Ortiz, J. T. L. Navarrete, S. Li, J. Strzalka, L. X. Chen, R. P. H. Chang, A. Facchetti and T. J. Marks, Polymer solar cells with enhanced fill factors, *Nat. Photonics*, 2013, **7**, 825.

65 M.-H. Jao, H.-C. Liao and W.-F. Su, Achieving a high fill factor for organic solar cells, *J. Mater. Chem. A*, 2016, **4**, 5784–5801.

66 G. Li, V. Shrotriya, Y. Yao and Y. Yang, Investigation of annealing effects and film thickness dependence of polymer solar cells based on poly(3-hexylthiophene), *J. Appl. Phys.*, 2005, **98**, 043704.

67 H.-C. Liao, C.-C. Ho, C.-Y. Chang, M.-H. Jao, S. B. Darling and W.-F. Su, Additives for morphology control in high-efficiency organic solar cells, *Mater. Today*, 2013, **16**, 326–336.

68 J. T. Rogers, K. Schmidt, M. F. Toney, E. J. Kramer and G. C. Bazan, Structural Order in Bulk Heterojunction Films Prepared with Solvent Additives, *Adv. Mater.*, 2011, **23**, 2284–2288.

69 C. Du, Y. Ji, J. Xue, T. Hou, J. Tang, S.-T. Lee and Y. Li, Morphology and Performance of Polymer Solar Cell Characterized by DPD Simulation and Graph Theory, *Sci. Rep.*, 2015, **5**, 16854.

70 Y.-A. Su, W.-C. Lin, H.-J. Wang, W.-H. Lee, R.-H. Lee, S. A. Dai, C.-F. Hsieh and R.-J. Jeng, Enhanced photovoltaic performance of inverted polymer solar cells by incorporating graphene nanosheet/AgNPs nanohybrids, *RSC Adv.*, 2015, **5**, 25192–25203.

71 J. Qi, X. Zhou, D. Yang, W. Qiao, D. Ma and Z. Y. Wang, Optimization of Solubility, Film Morphology and Photodetector Performance by Molecular Side-Chain Engineering of Low-Bandgap Thienothiadiazole-Based Polymers, *Adv. Funct. Mater.*, 2014, **24**, 7605–7612.

72 R.-H. Lee, J.-L. Huang and C.-H. Chi, Conjugated polymer-functionalized graphite oxide sheets thin films for enhanced photovoltaic properties of polymer solar cells, *J. Polym. Sci., Part B: Polym. Phys.*, 2013, **51**, 137–148.